中国光学（中英文） Chinese Optics 核心期刊

Cosh–Pearcey–Gaussian涡旋光束在单轴晶体中的坡印廷矢量和角动量密度

梁梦婷 程科 舒凌云 廖赛 杨嶒浩 黄宏伟

The poynting vector and angular momentum density of Cosh-Pearcey-Gaussian vortex beams in uniaxial crystals

LIANG Meng-ting, CHENG Ke, SHU Ling-yun, LIAO Sai, YANG Ceng-hao, HUANG Hong-wei

引用本文:
梁梦婷, 程科, 舒凌云, 廖赛, 杨嶒浩, 黄宏伟. Cosh–Pearcey–Gaussian涡旋光束在单轴晶体中的坡印廷矢量和角动量密度[J]. 中国光学, 2023, 16(1): 193–201. doi: 10.37188/CO.EN.2022–0007
LIANG Meng-ting, CHENG Ke, SHU Ling-yun, LIAO Sai, YANG Ceng-hao, HUANG Hong-wei. The poynting vector and angular momentum density of Cosh-Pearcey-Gaussian vortex beams in uniaxial crystals[J]. *Chinese Optics*, 2023, 16(1): 193-201. doi: 10.37188/CO.EN.2022-0007

在线阅读 View online: https://doi.org/10.37188/CO.EN.2022–0007

文章编号　2097-1842(2023)01-0193-09

The poynting vector and angular momentum density of Cosh-Pearcey-Gaussian vortex beams in uniaxial crystals

LIANG Meng-ting, CHENG Ke*, SHU Ling-yun, LIAO Sai, YANG Ceng-hao, HUANG Hong-wei
(*College of Optoelectronic Engineering*, *Chengdu University of Information Technology*, *Chengdu* 610225, *China*)
* *Corresponding author*, *E-mail*: *ck@cuit.edu.cn*

Abstract: We investigate a family of Cosh-Pearcey-Gaussian Vortex (CPeGV) beams, obtain the general propagation expressions of a CPeGV beam, and study the longitudinal and transverse Poynting vector and Angular Momentum Density (AMD) when the CPeGV beams propagate in uniaxial crystals. The effects of the cosh modulation parameter, topological charge, and propagation distance on the propagation properties of CPeGV beams are discussed. A larger cosh modulation parameter can lead the energy transfer significantly along the transverse Poynting vector direction. Moreover, we also investigate how the cosh modulation parameter and topological charge influence the propagation properties in the far-field. A larger cosh modulation parameter can lead AMD to present four-lobe structures rather than their usual parabolic curve. Our investigation will provide a better understanding of the state of the CPeGV beams propagating in uniaxial crystals and be useful for applications in information transmission.

Key words: Cosh-Pearcey-Gaussian vortex beams; Poynting vector; angular momentum density; uniaxial crystals

Cosh-Pearcey-Gaussian 涡旋光束在单轴晶体中的坡印廷矢量和角动量密度

梁梦婷, 程　科*, 舒凌云, 廖　赛, 杨嶒浩, 黄宏伟
(成都信息工程大学 光电工程学院, 四川 成都 610225)

摘要: 为了分析和研究 Cosh-Pearcey-Gaussian 涡旋 (CPeGV) 光束的传播特性, 通过皮尔斯积分式得到了 CPeGV 光束传播的一般表达式, 推导出 CPeGV 光束在单轴晶体中传播的解析式。详细研究了 CPeGV 光束在单轴晶体中传播时的纵向和横向坡印廷矢量和角动量密度 (AMD)。探讨了双曲余弦参数、拓扑电荷和传播距离对 CPeGV 光束传播特性的影响。研究结果表明: 与 PeG 光束相比, CPeGV 光束的调制自由度更高。较大的双曲余弦调制参数可以控制能量沿横向坡印廷矢量方向传递, 从而不仅可以改变能量分布也可以使 AMD 峰值变大。在远场, CPeGV 光束的纵向

收稿日期: 2022-04-14; **修订日期:** 2022-04-21
基金项目: 四川省科技计划资助项目(No. 23NSFSC1097)
Supported by Sichuan Science and Technology Program (No. 23NSFSC1097)

坡印廷矢量随着双曲余弦参数的增大会从抛物线形状分离为四个波瓣的分布形状。而拓扑电荷会影响远场抛物线形状中暗区的数量。本文研究将有助于更好地理解 CPeGV 光束在单轴晶体中的传播特性，并有助于信息传输和存储的应用。

关 键 词: Cosh-Pearcey-Gaussian 涡旋光束；坡印廷矢量；角动量密度；单轴晶体

中图分类号: TN929.1; **文献标志码:** A **doi:** 10.37188/CO.EN.2022-0007

1 Introduction

The Pearcey beams, based on the Pearcey function, were firstly studied by Pearcey in 1946[1]. In 2012, Ring *et al*. discovered experimentally that Pearcey beams include these propagation properties: autofocusing, form-invariance, and self-healing[2]. Due to the fact that Pearcey beams contain infinite energy[2], scientists tend to add the Gaussian factor to derive the more physical Pearcey Gaussian beams (PGBs), which contain finite energy. The unique properties of PGBs and Pearcey Gaussian Vortex Beams (PGVBs) such as their propagation properties and vectorial structures have been revealed by some researchers. For instance, in 2019, Deng *et al*. introduced a kind of PGBs with an astigmatic phase (APPGBs)[3], which reveals the rotating factor can rotate the transverse intensity distribution of the APPGBs on propagation in a chiral medium. Afterward, the effects of the multi-order and off-axis vortex on the propagation of PGVBs in a chiral medium were illustrated by Deng *et al*. in 2021[4]. As indicated in Refs. [5-8], Pearcey beams can be useful in multi microparticle manipulation[5], human tissue medicine, particle guiding[6], optical imaging, and optical trapping[7].

It is also interesting to investigate the propagation of beams in uniaxial crystals. As we know, laser beams propagating in uniaxial crystals can be applied effectively to determine the crystal structure and investigate the available optical phenomena of uniaxial crystals. Uniaxial crystal plays a significant role in the optimal design of polarizers, compensators, and amplitude and phase-modulation devices[8-9]. According to the current resources available, there are some research reports about Airy Gaussian beams[10], Airy vortex beams[11], and Pearcey beams[12] in uniaxial crystals, which show the influence of the anisotropic and refractive index on laser beam propagation.

Cosh-Airy beams, which have more manipulation degrees of freedom than the corresponding Airy beams, have been proposed, and the self-healing ability of the cosh-Airy beam was found be higher than that of the corresponding Airy beam in 2019[13]. To the best of our knowledge, energy flux distributions could be changed by cosh parameters and we cannot find more details about the vector properties of Cosh-Pearcey-Gaussian Vortex (CPeGV) beams. We introduce the cosh function to Pearcey-Gaussian vortex optical field in this paper, and it is natural to ask whether CPeGV beams can show more distinctive properties propagating in uniaxial crystals than in corresponding PeGV beams.

The purpose of this paper is to discuss the longitudinal and transverse Poynting vector and Angular Momentum Density (AMD) of CPeGV beams propagating in uniaxial crystal. We explore the influence of the topological charge on the Poynting vector in the far-field. Furthermore, we find the Fourier spectrum, the Poynting vector and how the energy flux distributions can be changed by properly selecting the cosh parameter during the propagating distance. Therefore, the propagation properties of the CPeGV beams in uniaxial crystals are more abundant than those of the corresponding PeGV beams. This research is beneficial to the practical applications of the CPeGV beams in many fields such as information storage and optical trapping particles.

2 Cosh-Pearcey-Gauss vortex beams

The input plane is z=0 and the observation plane is z. The ordinary and extraordinary refractive indices of the uniaxial crystal are n_o and n_e, respectively. The relative dielectric tensor of the uniaxial crystal reads as[12]

$$\varepsilon\begin{bmatrix} n_e^2 & 0 & 0 \\ 0 & n_o^2 & 0 \\ 0 & 0 & n_o^2 \end{bmatrix}, \tag{1}$$

In the Cartesian coordinate system, the transverse electric field of a CPeGV beam with off-axis optical vortices in the input plane z =0 is written as

$$\begin{pmatrix} E_x(x,y,0) \\ E_y(x,y,0) \end{pmatrix} = \begin{pmatrix} (x+i\mathrm{sgn}(m)Qy^{|m|})PeG(x,y,z=0)\cosh(\Omega x)\cosh(\Omega y) \\ 0 \end{pmatrix}. \tag{2}$$

The Pearcey-Gauss background beam in Eq. (2) is expressed as [14]

$$PeG(x,y,0) = \exp\left[-\frac{x^2+y^2}{w_0}\right]\times\int_{-\infty}^{\infty}\left\{i\left[s^4+s^2\left(\frac{y}{y_0}\right)+s\left(\frac{x}{x_0}\right)\right]\right\}\mathrm{d}s, \tag{3}$$

where Pe(x/x_0, y/y_0) is the Pearcey function with scaling lengths x_0 and y_0 along the x- and y-axes, respectively. To ensure the finite energy in real space, the Pearcey function is also modulated by a Gaussian factor with a waist width of w_0, m is the topological charge or order number of the embedded optical vortex at z=0, sgn (m) is the sign function, the complex parameter Q is the noncanonical strength of the embedded optical vortex and for Q=±1 the Eq. (2) is simplified to the canonical or symmetric vortex. Ω denotes the modulation parameter related to the cosh part.

The two-dimensional Fourier transforms is given by[15].

$$\tilde{F}_j(k_x,k_y) = \frac{1}{(2\pi^2)}\int_{-\infty}^{\infty}\int_{-\infty}^{\infty}E_j(x,y,0)\times\exp[-i(k_x x+k_y y)]\mathrm{d}x\mathrm{d}y, \tag{4}$$

where j is x or y. Substituting Eq. (2) into Eq. (4), we obtain the two-dimensional Fourier transform of the initial electric field of CPeGV beams as

$$\tilde{F}_x(k_x,k_y) = \frac{w_0^4}{4\pi}\times\sum_{s=1}^{2}\sum_{t=1}^{2}\left(\begin{array}{l}\exp\left[\frac{w_0^2}{4}(\Omega+(-1)^s ik_x)^2+\frac{w_0^2}{4}(\Omega+(-1)^s ik_y)^2\right]\times \\ \left[\left(a+\frac{(-1)^{s+1}\Omega}{2}\right)\varepsilon Pe(K_{xs},K_{yt})+iQ\left(b+\frac{(-1)^{t+1}\Omega}{2}\right)\varepsilon Pe(K_{x1},K_{y1})\right]\end{array}\right), \tag{5}$$

where

$$a=\frac{is}{2x_0}-\frac{ik_x}{2}, b=\frac{is^2}{2y_0}-\frac{ik_y}{2}, \varepsilon=\left(1+\frac{iw_0^2}{4y_0^2}\right),$$

and

$$K_{xs}=\frac{w_0^2\left((-1)^{s+1}\Omega-ik_x\right)}{2x_0}\varepsilon^{-\frac{1}{4}},$$

$$K_{yt}=\left(\frac{w_0^2\left((-1)^{t+1}\Omega-ik_y\right)}{2y_0}+\frac{iw_0^2}{4x_0^2}\right)\varepsilon^{-\frac{1}{2}}, (s,t=1,2),$$

Within the framework of the paraxial approximation, the propagation of the CPeGV beams in uniaxial crystals orthogonal to the optical axis obeys the following equations[10]:

$$E_x(x,y,z) = \frac{-\mathrm{i}kn_o}{2\pi z}\exp(\mathrm{i}kn_e z)\int_{-\infty}^{\infty}\int_{-\infty}^{\infty}E_x(x,y,0)\times \exp\left\{\frac{\mathrm{i}k}{2zn_e}[n_o^2(x-x_1)+n_e^2(y-y_1)]\right\}, \tag{6}$$

where $k = 2/\lambda$ is the wavenumber and λ is the optical wavelength, $z_e = 2ky_0^2$ and z is the propagation distance. Substituting Eqs. (1) and (2) into Eq. (6), and using the integral formulas

$$\int_{-\infty}^{\infty}x^n\exp\left(-px^2+2qx\right)\mathrm{d}x = n!\left(\frac{q}{p}\right)^n\sqrt{\frac{\pi}{p}}\exp\left(\frac{q^2}{p}\right)\times\sum_{k=0}^{n/2}(1/k!(n-2k))!\left(p/4q^2\right)^2. \tag{7}$$

Therefore, the propagating form of the CPeGV beams in uniaxial crystals is

$$E_x(x,y,z)=\frac{kn_o}{8iz\sqrt{p_1p_2}}\exp(ikn_ez)\exp\left[\frac{ik}{2zn_e}\left(n_o^2x^2+n_e^2y^2\right)\right]\times$$

$$\sum_{s=1}^{2}\sum_{t=1}^{2}\left(\begin{array}{l}\exp\left[\frac{1}{4p_1}\left(\Omega+\frac{(-1)^s ikn_o{}^2x}{zn_e}\right)^2+\frac{1}{4p_2}\left(\Omega+\frac{(-1)^t ikn_ey}{z}\right)^2\right]\times\\ \left[\frac{1}{p_1}\left(A+\frac{(-1)^{s+1}\Omega}{2}\right)\tau Pe(X_s,Y_t)+iQ\frac{1}{p_2}\left(B+\frac{(-1)^{t+1}\Omega}{2}\right)\tau Pe(X_s,Y_t)\right]\end{array}\right) . \quad (8)$$

where

$$P_1=\frac{1}{w_0{}^2}-\frac{ikn_o{}^2}{2zn_e},P_2=\frac{1}{w_0{}^2}-\frac{ikn_e}{2z},$$

$$A=\frac{is}{2x_0}-\frac{ikn_o{}^2x}{2zn_e},B=\frac{is^2}{2y_0}-\frac{ikn_ey}{2z},\tau=1+\frac{i}{4P_2y_0{}^2} ,$$

and

$$X_s=\frac{(-1)^{s+1}\Omega-\frac{ikn_o{}^2x}{zn_e}}{2P_2x_0}\tau^{-\frac{1}{4}},$$

$$Y_t=\left(\frac{(-1)^{t+1}\Omega-\frac{ikn_ey}{z}}{2P_2y_0}+\frac{i}{4P_1x_0{}^2}\right)\tau^{-\frac{1}{2}},(s,t=1,2) ,$$

Figure 1 shows the dependence of the Fourier spectrum of the CPeGV beam on cosh modulation parameter Ω and topological charge *m*. One can see that their spectra present parabola structures and they can be partitioned by cosh parameter Ω and topological charge *m*. The maximal values are located on two sides rather than the vertex of a parabola as shown in the i and iii figures in Fig.1 (a) (color online). A larger Ω or *m* can lead to a growth in the number of partitioned side-lobes, and an increase in their maximal values in the Fourier spectrum as shown in iv of Fig.1 (a) and 1 (b) (color online), by comparing ii in Fig.1 (a) and in Fig.1 (b), it can be seen that the number of partitioned side-lobes in Ω=5 is significantly greater than that of Ω=2 in the case of equal *m*, which indicates that the cosh parameter Ω has an advantage over topological charge *m* in the ability of partitioned side-lobes.

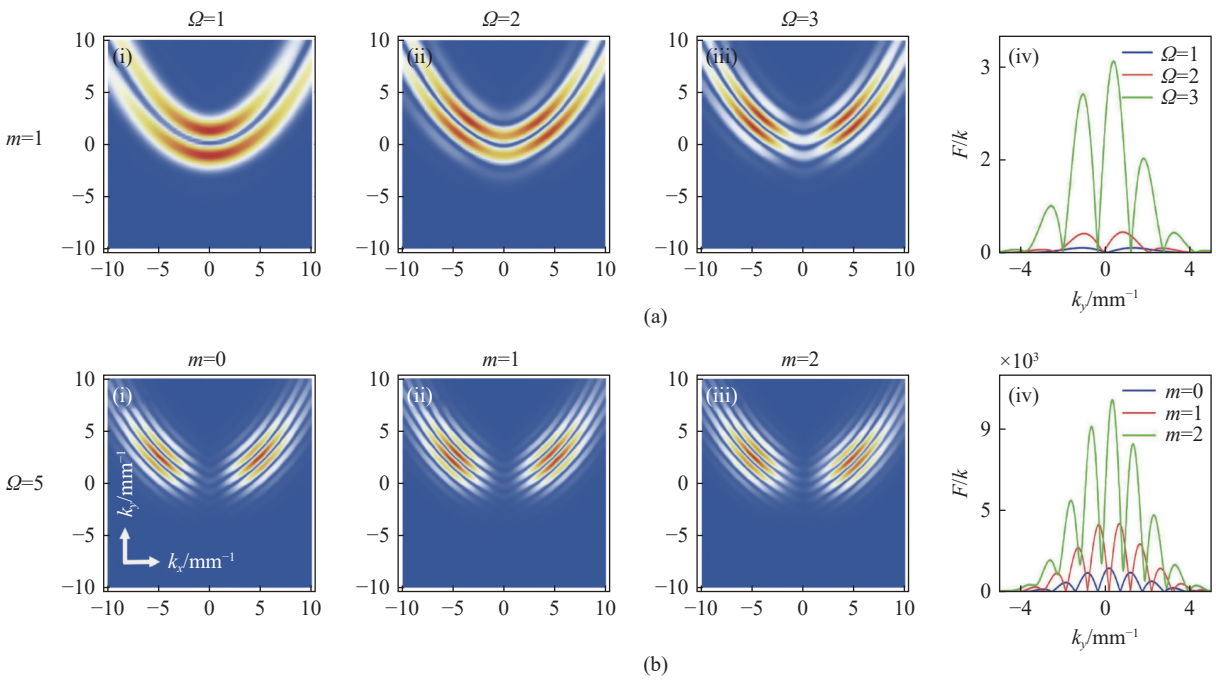

Fig. 1 The dependence of Fourier spectrum of CPeGV beams on cosh modulation parameter Ω and topological charge *m*; (a) the topological charge *m*= 1; (b) the cosh modulation parameter Ω=5.

3 The Poynting vector and angular momentum density of CPeGV

In the paraxial domain, the time-averaged Poynting vector[16] of the optical wave field in a Cartesian coordinate is defined as

$$\langle \boldsymbol{S}\rangle = \frac{c}{4\pi}\langle \boldsymbol{E}\times\boldsymbol{H}\rangle = \frac{c}{4\pi}\times\frac{1}{2}\boldsymbol{Re}(\boldsymbol{E}^*\times\boldsymbol{H}) = \frac{c}{4\pi}\left\{\frac{iw}{2}\left[\left(E\frac{\partial E^*}{\partial x}-E^*\frac{\partial E}{\partial x}\right)\boldsymbol{e}_x+\left(E\frac{\partial E^*}{\partial y}-E^*\frac{\partial E}{\partial y}\right)\boldsymbol{e}_y\right]+wk|E|^2\boldsymbol{e}_z\right\} = \frac{c}{4\pi}(S_x\boldsymbol{e}_x+S_y\boldsymbol{e}_y+S_z\boldsymbol{e}_z) \quad , \tag{9}$$

where $\boldsymbol{E}$ and $\boldsymbol{H}$ represent the electric and magnetic field vectors, respectively, c is the speed of light, w stands for circular frequency $k=2\pi/\lambda$ is the wave-number, and the asterisk denotes complex conjugation. The S_x, S_y, and S_z are the x-, y- and z components of the time-averaged Poynting vector, respectively, and their values are real. The Poynting vector describes the rate of electromagnetic energy flow per unit area, and the z-component of the Poynting vector is proportional to the light intensity.

The AMD of the electromagnetic field $\boldsymbol{J}$ is related to the linear momentum density P by $\boldsymbol{J}= r \times \boldsymbol{P}$[17], where r is the position vector and the linear momentum density is proportional to the Poynting vector. Therefore, the time-averaged AMD can be expressed as[18]

$$\langle \boldsymbol{J}\rangle = r\times\langle \boldsymbol{E}\times\boldsymbol{H}\rangle = J_x e_x + J_y e_y + J_z e_z \quad , \tag{10}$$

$$J_x = yS_z - zS_y = ywk|E|^2 - \frac{iwz}{2}\left(E\frac{\partial E^*}{\partial y}-E^*\frac{\partial E}{\partial y}\right) \quad , \tag{11}$$

$$J_y = zS_x - xS_z = \frac{iwz}{2}\left(E\frac{\partial E^*}{\partial x}-E^*\frac{\partial E}{\partial x}\right) - xwk|E|^2 \quad , \tag{12}$$

$$J_z = xS_y - yS_x = \frac{iw}{2}\left[x\left(E\frac{\partial E^*}{\partial y}-E^*\frac{\partial E}{\partial y}\right)-y\left(E\frac{\partial E^*}{\partial x}-E^*\frac{\partial E}{\partial x}\right)\right] \quad . \tag{13}$$

3.1 The transverse and longitudinal Poynting vector

Figure 2 (color online) shows the evolution of the longitudinal and transverse Poynting vectors of the CPeGV beams in uniaxial crystals, where the direction and length of the arrows denote the direction and magnitude of the transverse Poynting vector. It is found that auto-focusing and inversion are still maintained, and the far-field pattern presents parabolic structures with dark lines. The original en-

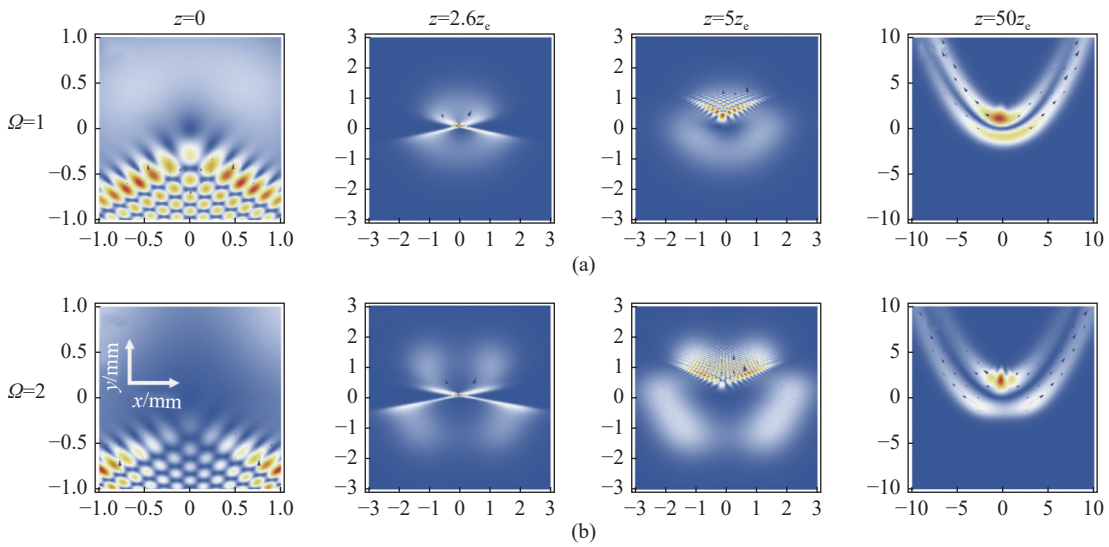

Fig. 2 The intensity (backgrounds) and the transverse Poynting vector (arrows) of the CPeGV beams propagating in uniaxial crystal for different propagation distances z with different cosh modulation parameters Ω and n_e=1.2n_o; (a): Ω=1; (b): Ω=2 and m=1.

ergy of CPeGV beams concentrates on side lobes due to the vortex core and the cosh parameter, which is different from the concentrated energy on the main lobes of the Pearcey beams. The direction of the transverse Poynting vector moves from side-lobes to the main lobes, but their direction is opposite beyond the auto-focusing plane. Moreover, the energy flux flows from the vertex to the two sides of the parabola along the optical intensity channels, and the deviation of the optical bright spot can be found owing to anisotropy.

Figure 3 (color online) depicts the longitudinal and transverse Poynting vectors of the CPeGV beams for different cosh modulation parameters Ω and topological charges m at z=300 z_e. One can see that the number of partitioned side-lobes with a parabolic structure increases as cosh modulation parameter Ω and topological charge m increase. The main lobe near the origin gradually disappears with an increase of cosh modulation parameter Ω and further presents four-lobe structures rather than the usual parabolic curves. For the embedded optical vortex with topological charge m=+2, the far-field optical vortex can be also found and marked by a white "×". Specifically, it can be seen their locations are (0.11,15.91) for Ω=3, and (2.91,−1.73), (4.88,−0.88) for Ω=5 and (−2.35,0.2), (−1.6,−0.5) and (0.06,−1.9) for Ω=9 respectively.

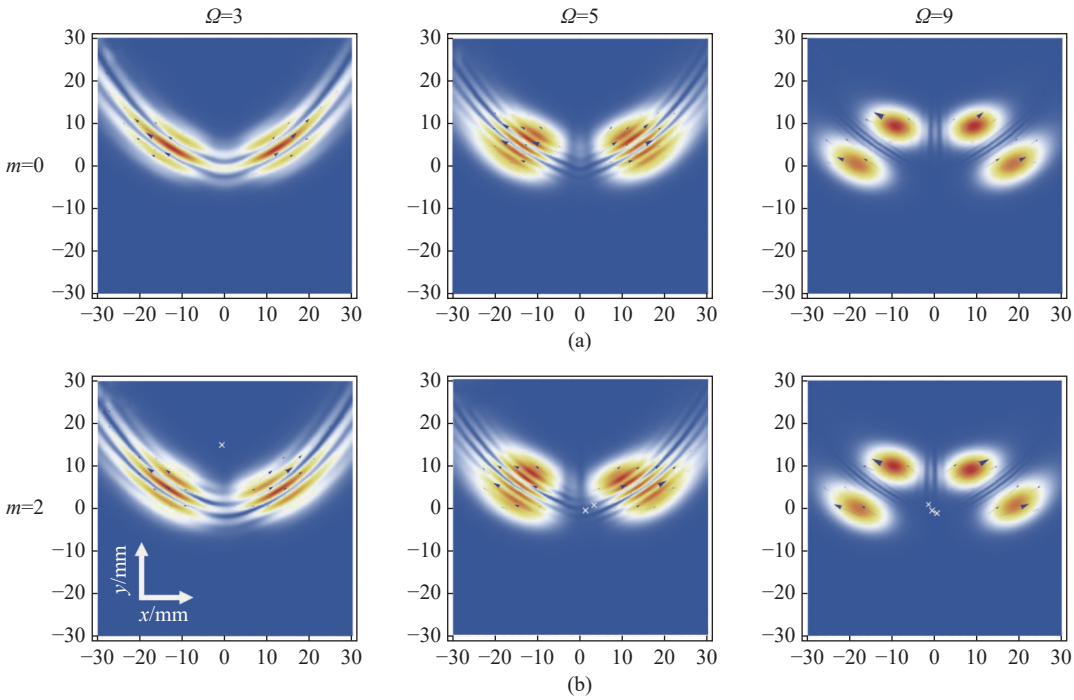

Fig. 3 The longitudinal and transverse Poynting vectors of the CPeGV beams for different cosh modulation parameters Ω and topological charges m at z=300z_e. (a): m=0; (b): m=2.

3.2 The transverse and longitudinal angular momentum density

To further describe the evolution of AMD, the dependencies of the z-component, x-component, and y-component of the AMD of the beam on cosh modulation parameter Ω, topological charge m, and propagation distance z are shown in Figures 4 to 6 (color online).

Figure 4 gives the evolution of the longitudinal AMD of the CPeGV beams in uniaxial crystal. Comparing the two figures in the first column of Fig. 4, we find that a greater Ω leads to the maximal rate of AMD increase. On the other hand, by observing the numerical value of the color bars, we find that the maximal value of AMD firstly increases and then decreases as z evolves, reaching a peak at the focusing plane. The longitudinal AMD of Fig.4 exhibits parabolic shapes (see the last

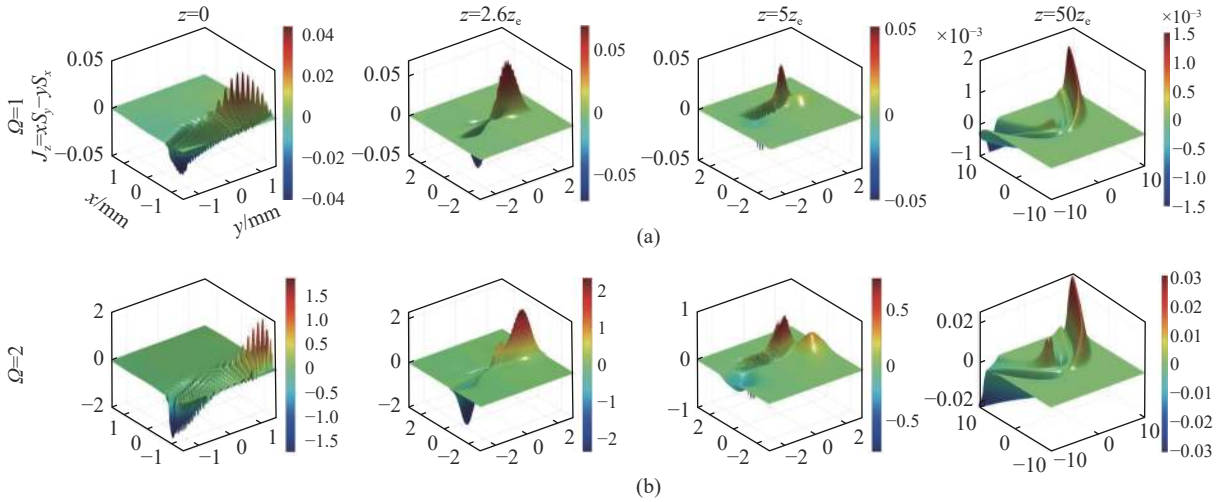

Fig. 4　The longitudinal AMD of the CPeGV beams propagating in uniaxial crystal for different propagation distances z with different cosh modulation parameters Ω and n_e=1.2n_o, m=1. (a): Ω=1; (b): Ω=2

column) at z=50 z_e. Furthermore, due to the embedded optical vortex, the splits in the positive direction are greater than those in the negative direction, which leads to the net AMD being positive. For example, the maximum values of the positive and negative directions are 0.044 2 and −0.04 at the input plane, respectively. This is because $\boldsymbol{J}=\boldsymbol{L}+\boldsymbol{S}$ and the linear polarization leads to $\boldsymbol{S}$=0, then the $\boldsymbol{J}$ will be positive or negative depending on the AMD. In other words, it's related to vortex properties. The net AMD is still positive in the far-field.

More details on the evolution of the maximum AMD of CPeGV beams in uniaxial crystals are shown in Fig. 5 (color online). Their maxima increase and reach peak values at the autofocusing plane, and a higher peak value is accompanied by a larger Ω. For example, their maxima in AMD densities are 0.083, 0.02, 0.03 for Ω=1, 2, and 3, respectively. The results indicate that the autofocusing properties not only appear in the evolution of the Poynting vector but also display in AMD densities.

Figure 6 (color online) describes the normalized longitudinal AMD of the CPeGV beams for different cosh modulation parameters Ω and topological charges m at z=300z_e. One can find that the AMD $\boldsymbol{J}_z$ tends to split more branches from the positive and negative direction of the z-axis with increases in the absolute value of topological charge

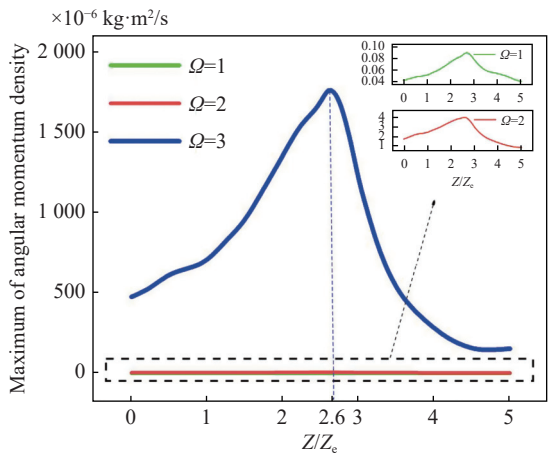

Fig. 5　Maximum of angular momentum density of CPeGV beams in uniaxial crystal for different propagation distances z with different cosh modulation parameters Ω

m. The splits in the positive direction are greater than those in the negative direction, which leads to the appearance of a positive AMD. However, a greater Ω leads to AMD presenting four side-lobe structures in the far-field rather than a parabolic structure. Compared with PeGV beams, CPeGV beams have one more regulatory parameter Ω. Therefore, it is easier to regulate and control the Poynting vector and AMD of the optical beam in uniaxial crystals. The results obtained here are beneficial to the design of a more reasonable compensator and polarizer.

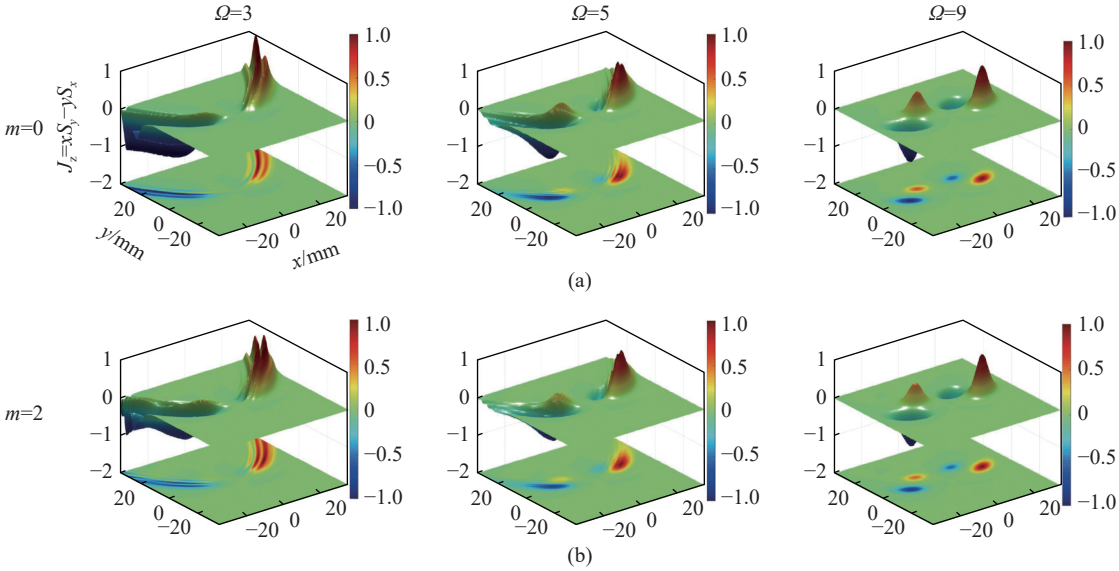

Fig. 6 The normalized AMD of the CPeGV beams in uniaxial crystal at $z=300z_e$ for different cosh modulation parameters Ω with different topological charges and $n_e=1.2n_o$; (a): $m=0$; (b): $m=2$

4 Conclusion

The propagation properties of CPeGV beams are numerically demonstrated in uniaxial crystals. The effects of Ω variation and topological charge variation on Poynting vector and AMD in uniaxial crystal propagation and far-field stability are investigated. Although all parameters have effects on the intensity pattern and the energy distribution of CPeGV beams, the main roles they play are different. The results show that the CPeGV beams still exhibit self-focusing and reversal properties with an increase in propagation distance during the propagation of uniaxial crystal. The energy distribution of the CPeGV beams can be changed by Ω, where energy might shift to a side lobe. Moreover, the longitudinal Poynting vector first presents a parabolic shape in the far-field, which can be explained by the direction of the arrow of the transverse Poynting vector. With an increase in Ω, the longitudinal Poynting vector will converge along the direction of the transverse Poynting vector, and finally, become four-lobes structures. Along with the propagation distance, the trend of change to the maximum AMD is to first increase and then decrease. Moreover, as the Ω increases, the peak value of AMD also increases significantly. Our investigation will provide a better understanding of the state of CPeGV beams propagating in uniaxial crystal and be useful for applications in information transmission.

References:

[1] PEARCEY T. XXXI. The structure of an electromagnetic field in the neighbourhood of a cusp of a caustic[J]. *The London, Edinburgh, and Dublin Philosophical Magazine and Journal of Science*, 1946, 37(268): 311-317.

[2] RING J D, LINDBERG J, MOURKA A, *et al*.. Auto-focusing and self-healing of Pearcey beams[J]. *Optics Express*, 2012, 20(17): 18955-18966.

[3] ZENG Z SH, DENG D M. Paraxial propagation of Pearcey Gaussian beams with the astigmatic phase in the chiral medium[J]. *Journal of the Optical Society of America B*, 2020, 37(1): 30-37.

[4] HUANG ZH C, WU Y, LIN Z J, *et al*.. Effects of the multi-order and off-axis vortex on the propagation of Pearcey Gaussian vortex beams with the astigmatic phase in a chiral medium[J]. *Waves in Random and Complex Media*, 2021: 1-11.

[5] JIANG J J, MO ZH W, XU D L, *et al*.. Elliptical Pearcey beam[J]. *Optics Communications*, 2022, 504: 127475.

[6] WU Y, ZHAO J J, LIN Z J, *et al*.. Symmetric Pearcey Gaussian beams[J]. *Optics Letters*, 2021, 46(10): 2461-2464.

[7] LIU Y J, XU CH J, LIN Z J, *et al*.. Auto-focusing and self-healing of symmetric odd-Pearcey Gauss beams[J]. *Optics Letters*, 2020, 45(11): 2957-2960.

[8] CIATTONI A, CINCOTTI G, PALMA C. Propagation of cylindrically symmetric fields in uniaxial crystals[J]. *Journal of the Optical Society of America A*, 2002, 19(4): 792-796.

[9] CIATTONI A, PALMA C. Optical propagation in uniaxial crystals orthogonal to the optical axis: paraxial theory and beyond[J]. *Journal of the Optical Society of America A*, 2003, 20(11): 2163-2171.

[10] ZHOU M L, CHEN CH D, CHEN B, *et al*.. Propagation of an Airy-Gaussian beam in uniaxial crystals[J]. *Chinese Physics B*, 2015, 24(12): 124102.

[11] DENG D M, CHEN CH D, ZHAO X, *et al*.. Propagation of an Airy vortex beam in uniaxial crystals[J]. *Applied Physics B*, 2013, 110(3): 433-436.

[12] XU CH J, LIN L D, HUANG ZH ZH, *et al*.. Propagation of a Pearcey beam in uniaxial crystals[J]. *Chinese Physics B*, 2019, 28(2): 024201.

[13] ZHOU G Q, CHEN R P, CHU X X. Propagation of cosh-Airy beams in uniaxial crystals orthogonal to the optical axis[J]. *Optics & Laser Technology*, 2019, 116: 72-82.

[14] XU CH J, WU J H, WU Y, *et al*.. Propagation of the Pearcey Gaussian beams in a medium with a parabolic refractive index[J]. *Optics Communications*, 2020, 464: 125478.

[15] LIAN M, GU B, ZHANG Y D, *et al*.. Polarization rotation of hybridly polarized beams in a uniaxial crystal orthogonal to the optical axis: theory and experiment[J]. *Journal of the Optical Society of America A*, 2017, 34(1): 1-6.

[16] SZTUL H I, ALFANO R R. The Poynting vector and angular momentum of Airy beams[J]. *Optics Express*, 2008, 16(13): 9411-9416.

[17] ALLEN L, PADGETT M J. The Poynting vector in Laguerre-Gaussian beams and the interpretation of their angular momentum density[J]. *Optics Communications*, 2000, 184(1-4): 67-71.

[18] CHENG K, ZHOU Y, LU G, *et al*.. Vectorial structures of linear-polarized Butterfly-Gauss vortex beams in the far zone[J]. *Optics Communications*, 2018, 415: 107-114.

Author Biographics:

Mengting Liang (1997—), female, was born in Zigong, Sichuan province, M. Phil, College of Optoelectronic Engineering, Chengdu University of Information Technology. Her research interests are in the propagation and control of high-power lasers. E-mail: m1389008324@163.com

Cheng Ke (1979—), male, was born in Jianli, Hubei province, Ph. D, Professor, College of Optoelectronic Engineering, Chengdu University of Information Technology. His research interests are in the propagation and control of high-power lasers. E-mail: ck@cuit.edu.cn